Study of the 1D Scattering Mechanisms' Impact on the Mobility in Si Nanowire Transistors

C. Medina-Bailon*†, T. Sadi‡, M. Nedjalkov§, J. Lee†, S. Berrada†, H. Carrillo-Nunez†, V. Georgiev†, S. Selberherr§ and A. Asenov†

† School of Engineering, University of Glasgow, Glasgow G12 8LT, Scotland, UK

‡ Department of Neuroscience and Biomedical Engineering, Aalto University, P.O. Box 12200, FI-00076 Aalto, Finland

§ Institute for Microelectronics, TU-Vienna, Gußhausstraße 27-29, E360 A-1040, Vienna, Austria

* e-mail: Cristina.MedinaBailon@glasgow.ac.uk

***Abstract*—The extensive research of aggressively scaled nanoelectronic devices necessitates the inclusion of quantum confinement effects and their impact on performance. This work implements a set of multisubband phonon and impurity scattering mechanisms and the Kubo-Greenwood theory in order to study their impact on the mobility in Si nanowire transistors (NWTs). This 1D treatment has been coupled with a 3D Poisson-2D Schrödinger solver, which accurately captures the effect of confinement on charge dynamics. We also emphasize the importance of using the 1D models to evaluate the geometrical properties on mobility at the scaling limit.**

***Index Terms*—Phonon Scattering; Impurity Scattering; Kubo-Greenwood Formalism; Matthiessen rule; Nanowire FETs**

I. Introduction

Nanowire transistors (NWTs) are being considered as candidates for replacing FinFETs in aggressively scaled CMOS technology due to their better electrostatic integrity. In particular, NWTs are presented as an extension for CMOS scaling down to the 7-nm node [1]. In the corresponding simulation technologies, the reduction of the characteristic confined dimensions increases the importance of including quantum mechanical effects. Accordingly, it has been mandatory to develop different schemes in order to reduce the computational effort of these quantum transport mechanisms. One of the most popular approaches is to incorporate the important quantum effects into semi-classical simulator models with refined macroscopic quantities. The low-field electron mobility is one of the most important parameters that determines the performance potential of NWTs [2], and so its study in novel computational techniques represents an area of interest.

The approach considered herein combines quantum effects with the semi-classical Boltzmann transport equation (BTE) in the relaxation time approximation of 1D electron gas adopting the Kubo-Greenwood formalism [3]–[5]. This strategy delivers reliable mobility values at low-field near-equilibrium conditions, based on the rates of the relevant scattering mechanisms governing multisubband transistors in NWTs [6]. Then, the cumulative effect of the scattering probabilities are calculated by applying the Matthiessen's rule [7]. This combined semi-classical strategy allows the computation of each mechanism separately due to the probability based Matthiessen's rule. In contrast, purely quantum transport theories involve phases and amplitudes and so they preclude a separate treatment of the involved physical factors. In this work, we study the effect of quantum confinement on the electron mobility in NWTs including phonon and impurity scattering. In addition, we analyze the impact of the nanowire size and geometry on the transport properties.

II. Methodology

Long-channel simulations provide a convenient framework for assessing low-field electron mobilities in devices with strong confinement effects, such as NWTs. It directly studies the effect of charge confinement on transport as a function of out-of-plane (lateral) applied low electric field. We have chosen this framework in order to pre-calculate the potential profile and the corresponding eigenvalues of the subbands in the NW cross section.

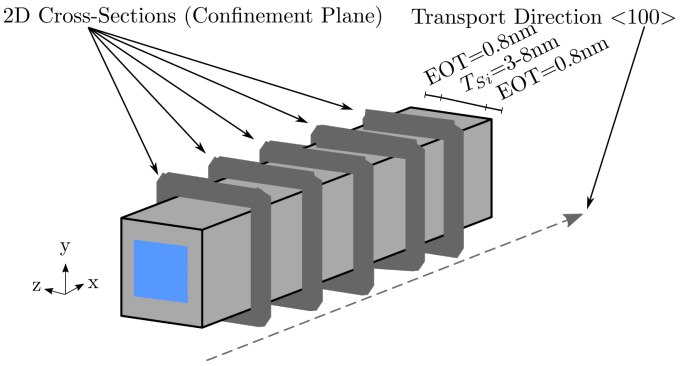

Fig. 1. NWT structures analyzed in this work with widths ranging from 3nm to 8nm. The coupled 2D Schrödinger and 3D Poisson equation are solved for each cross-section (confinament plane) and then the scattering rates are calculated accounting for the potential and the eigenfunctions for each subband.

For calculating the mobilities with the aforementioned assumption, some steps are needed in the simulation scheme. First, the channel is assumed to be infinitely long and the electric field in the transport direction is fixed to a low value (1kV/cm in this work). Second, multiple cross sections of the device are simulated using the coupled 3D Poisson and 2D Schrödinger solver (Fig. 1) integrated in the TCAD simulator GARAND from Synopsys [8]. Third, the potential and the corresponding eigenfunctions of the subbands are included in

the particular scattering rates, whose expressions have been directly developed from Fermi's Golden Rule accounting to the multi-subband quantization in the normal to the nanowire plane of confinement. These scattering mechanisms control the electron velocity and redistribute the electron densities between different subbands making the calculation of any macroparameters possible, in order to characterize the system. The total energy (E_l) of a (l, k_z) state is calculated as the sum of the kinetic energy $E_{Kin} = \frac{\hbar^2 k_z^2}{2m}$ and the energy level ($E_{subband}(l)$) of the subband l in which it is located. In this work, we have included:

(i) Acoustic Phonon Scattering. This model makes use of the short wave vector limit, in which energy is proportional to the averaged sound velocity $\bar{u}$. In addition, it has been characterized considering that: first, it is elastic, which means that the total energy of the initial (l, k_z) and the final (l', k_z') states must be the same ($E_l = E_{l'}$); and second, only intra-valley transitions are allowed.

(ii) Optical Phonon Scattering. In these transitions, the initial and final states can be located in different valleys and the involved phonons have a high momentum. Accordingly, this scattering model can be handled as the intra-valley acoustic one keeping in mind that the deformation potential and the involved phonon energy must be independent of $\vec{q}$ due to the short wave vector limit. Moreover, this mechanism is inelastic and so the final energy must satisfy $E_{l'} = E_l \pm \hbar\omega$ by absorbing or emitting a phonon. We have focused on Si NWs in this work and so the two different inter-valley transitions among the six equivalent X minimum of silicon must be considered: g-type and f-type processes whose transitions are made along the same line but opposite directions and happen among ∇ valleys along different directions, respectively. We have included fixed parameters for the different branches. In particular, for the $[100]$ direction herein analyzed, the set of X valleys are characterized by two-fold degeneracies. For instance, if the X1 valley is considered as the initial one, the g-type transitions set the X1 as the final valley and so it has been developed here as an intra-valley process. On the other hand, the final valleys in this example could be either X3 or X5 for f-type transitions.

(iii) Ionized Impurity Scattering. It is relevant for all types of doped nanostructures due to the short range Coulomb interaction with the carriers. This mechanisms only allows elastic and intra-valley transitions, and considers a fixed ionized impurity concentration $n_0 = 10^{19} cm^{-3}$. Fermi integrals are used to compute the charge density and the Debye Length. In this work, the former parameters have been re-calculated for each bias point including the effect of the new subbands and the quasi Fermi level.

Then, the mobilities are calculated by applying the Kubo-Greenwood formula to the relaxation times of 1D electron gas corresponding to the linearized BTE. In this approach, the quasi Fermi level, which is needed in the Kubo-Greenwood formula, is determined from the carrier concentration obtained from the 3D Poisson-2D Schrödinger solver. Finally, Matthiessen's rule is used to combine the scattering probabilities, and so both the individual and the total mobilities of the simulated device are analyzed separately. An important property of this semiclassical approach is the decomposition principle which, in turn, gets a feasible numerical procedure and so decreases the total computational time: the effects of different mechanisms can be independently modeled and then unified by the Mathiessen's rule into a general model.

III. Results and Discussion

The simulated device is a silicon gate-all-around (GAA) nanowire transistor (NWT) which has been parametrized for wire thickness and width from 3nm to 8nm and for square and circular device shapes. The rest of the technological parameters remains constant: the crystal orientation is [100], the gate oxide with Equivalent Oxide Thickness EOT=0.8nm, and the metal gate work function is set to 4.35eV. The gate bias is adjusted to obtain the sheet density reported in the following results. Table I shows effective masses corresponding to this [100] orientation, where x is the transport direction. Despite NWTs start to have a bulk-like behavior only at diameters higher than 8nm, we use bulk effective mass values.

Valley	m_x	m_y	m_z
X1	$m_l = 0.916m_0$	$m_t = 0.198m_0$	$m_t = 0.198m_0$
X3	$m_t = 0.198m_0$	$m_l = 0.916m_0$	$m_t = 0.198m_0$
X5	$m_t = 0.198m_0$	$m_t = 0.198m_0$	$m_l = 0.916m_0$

TABLE I
TRANSPORT (m_x) AND CONFINEMENT (m_y, m_z) EFFECTIVE MASSES IN THE [100] SILICON DEVICES FOR THE SET OF VALLEYS X1, X3 AND X5.

Figure 2 shows the energy levels for a square NW with the lowest diameter herein considered (3nm) and the largest one (8nm). The variation of the NW diameter includes a valley splitting energy leaving less final states for scatterings.

Fig. 3 presents the scattering rates as a function of the total energy for electrons calculated for impurity, acoustic phonon, and optical phonon (including f-, g-type and total) scatterings for a square NWT with 3nm (top) and 8nm (bottom) widths for a [100] orientation and 20 subbands. The multisubband effects in the scattering rates are generally more pronounced for smaller wire diameter. This is associated with the higher energy difference between the lower and upper subbands (Fig. 2), which minimizes the possible electron transitions between the subbands. In addition, it is important to highlight here that the overlap factor increases as the diameter is reduced because it is inversely proportional to the NW area. This results in a reduction of the mobility (both the individual and the total) for highly confined devices (Fig. 4). Moreover, for such

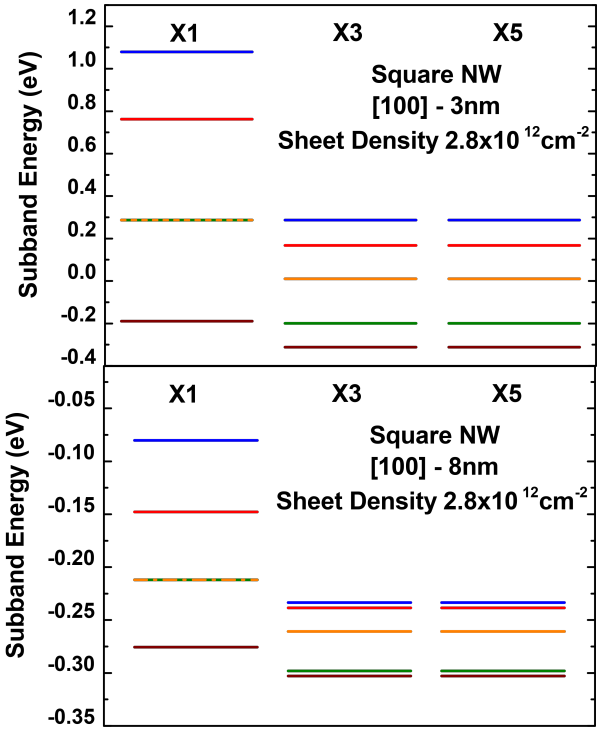

Fig. 2. Energy levels for a square NW with 3nm (top) and 8nm (bottom) width for [100] orientation and sheet density of $2.8 \times 10^{12}\ cm^{-2}$, showing band splitting for the set of valleys X1, X3 and X5.

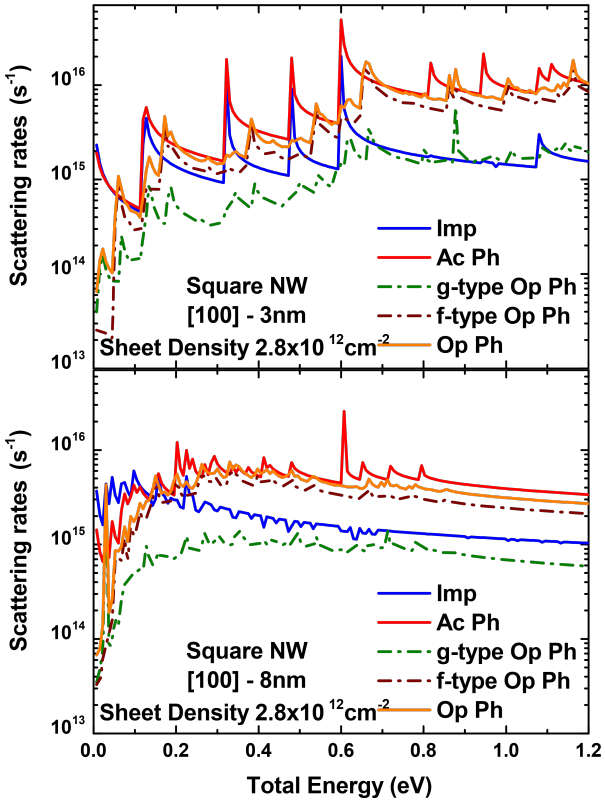

Fig. 3. Impurity scattering rate (Imp) as well as acoustic (Ac Ph), optical (including g-type, f-type and total (Op Ph)) phonon scattering rates as a function of the total energy for a square NW with 3nm (top) and 8nm (bottom) width for [100] orientation and sheet density of $2.8 \times 10^{12}\ cm^{-2}$.

devices and assuming a rather large impurity concentration, the mobility is limited by both the acoustic phonon and the ionized impurity scatterings due to its high scattering rates, especially at low energy (Fig. 4).

Finally, Fig. 5 shows the electron mobility considering only the impact of phonon scattering as well as both phonon and impurity scatterings of square and circular NWTs as a function of the cross section area. The latter affects directly the subband energy levels and eigenfunctions, as illustrated in Fig. 6 which shows the wavefunction of the first and second subbands (X3 valleys) for the 3nm and 8nm diameters for both square and circular NWs shape. Consequently, the direct impact on the change of these parameters modifies the overlap factor and so it may enhance or degrade the mobility substantially. Moreover, the results presented in Fig. 5 are in good agreement with our previous work [9] where we observed higher mobile charge in circular NW in comparison to the square device. As expected, the ionized impurity mechanism is the dominant one for such large impurity concentration $n_0 = 10^{19} cm^{-3}$ [10].

IV. Conclusions

This work presents the implementation of the Kubo-Greenwood theory including acoustic phonon, optical phonon, and impurity scattering mechanisms for the study of the mobility effect in Si nanoware transistors. In addition, the shape and dimension of the NWs have been also modified. The total mobility is calculating by means of the Matthiessen's rule as a function of the individual ones. This 1D simulation module is coupled with a commercial 3D Poisson-2D Schrödinger solver in order to pre-calculate the potential profile and the eigenvalues in the NWs. This works shows that the mobility increases for lower wire width NWs due to their higher multisubband effects in the scattering mechanisms. For these particular devices and and assuming a rather large impurity concentration, acoustic phonon and ionized impurity scattering presents the highest impact by controlling the total mobility due to its higher scattering rates. Moreover, we have demonstrated that the NWT shape has a strong impact on the potential profile and the corresponding eigenvalues. In conclusion, the circular NWTs is a better candidate for mobility performance for smaller devices.

V. Acknowledgment

The research leading to these results has received funding from the European Union's Horizon 2020 research and innovation programme under grant agreement No 688101 SUPERAID7. The authors would like to thank Dr. Ewan Towie for useful discussions.

References

[1] B. Yu, H. Wang, C. Yang, P. Asbeck, and Y. Taur, "Scaling of nanowire transistors," *IEEE Transactions on Electron Devices*, vol. 55, no. 11, pp. 2846 – 2858, 2008.

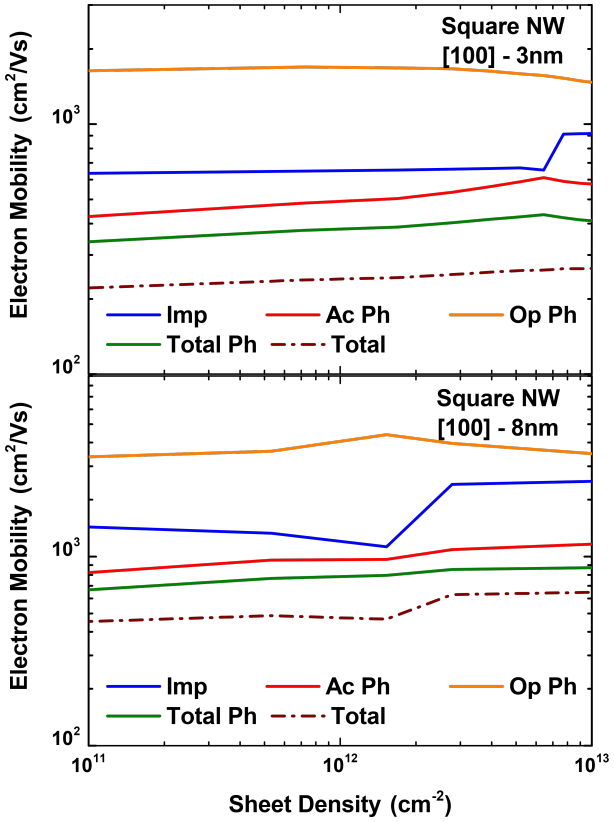

Fig. 4. Electron mobility as a function of the sheet density considering the impurity (Imp) as well as the acoustic (Ac Ph), optical (Op Ph), and total (Total Ph) phonon scattering separately as well as combined for a square NW with 3nm (top) and 8nm (bottom) width for [100] orientation.

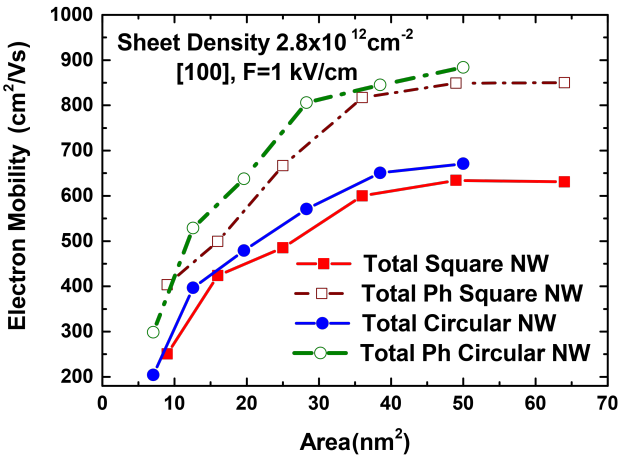

Fig. 5. Electron Mobility as a function of the area considering the impact of phonon (Total Ph) as well as both phonon and impurity scattering (Total) for a square and circular NW with sheet density of $2.8 \times 10^{12}\ cm^{-2}$.

[2] I. M. Tienda-Luna, F. G. Ruiz, A. Godoy, B. Biel, and F. Gámiz, "Surface roughness scattering model for arbitrarily oriented silicon nanowires," *Journal of Applied Physics*, vol. 110, no. 8, p. 084514, 2011.

[3] L. S. D. Esseni, P. Palestri, *Nanoscale MOS Transistors: Semi-classical Transport And Applications*. New York, USA: Cambridge University Press, 2011.

[4] D. Ferry and C. Jacoboni, *Quantum transport in semiconductors*. Berlin, Germany: Springer Science & Business Media, 1992.

[5] S. Jin, T.-W. Tang, and M. V. Fischetti, "Simulation of silicon nanowire transistors using boltzmann transport equation under relaxation time approximation," *IEEE Transactions on Electron Devices*, vol. 55, no. 3, pp. 727–736, 2008.

[6] S. Jin, M. V. Fischetti, and T.-W. Tang, "Modeling of electron mobility in gated silicon nanowires at room temperature: Surface roughness scattering, dielectric screening, and band nonparabolicity," *Journal of Applied Physics*, vol. 102, no. 8, p. 083715, 2007.

[7] D. Esseni and F. Driussi, "A quantitative error analysis of the mobility extraction according to the matthiessen rule in advanced mos transistors," *IEEE Transactions on Electron Devices*, vol. 58, no. 8, pp. 2415–2422, 2011.

[8] "Garand User Guide,https://solvnet.synopsys.com,Synopsys, Inc., 2017."

[9] Y. Wang, T. Al-Ameri, X. Wang, V. P. Georgiev, E. Towie, S. M. Amoroso, A. R. Brown, B. Cheng, D. Reid, C. Riddet, L. Shifren, S. Sinha, G. Yeric, R. Aitken, X. Liu, J. Kang, and A. Asenov, "Simulation study of the impact of quantum confinement on the electrostatically driven performance of n-type nanowire transistors," *IEEE Transactions on Electron Devices*, vol. 62, no. 10, pp. 3229–3236, 2015.

[10] N. Neophytou and H. Kosina, "Atomistic simulations of low-field mobility in si nanowires: Influence of confinement and orientation," *Physical Review B*, vol. 84, pp. 085 313 – 085 328.

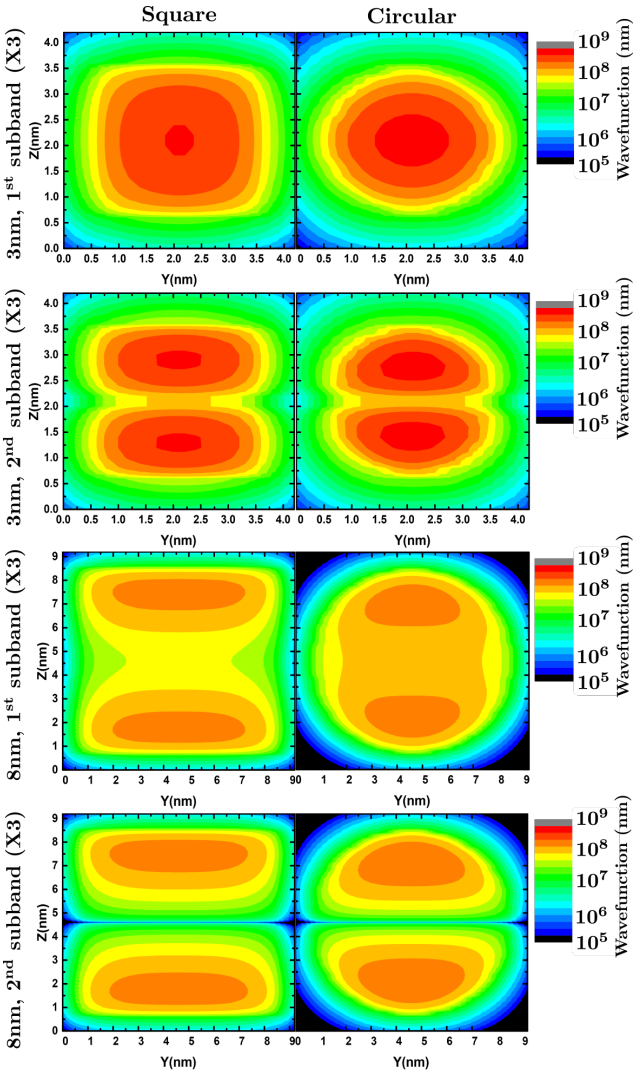

Fig. 6. Wavefunction of the first and second subbands (X3 valleys) for the 3nm and 8nm diameters for both square and circular NWs shape with sheet density of $2.8 \times 10^{12}\ cm^{-2}$.